

1 **From Bright Windows to Dark Spots: The Evolution of Melt Pond Optical**
2 **Properties during Refreezing**

3

4 **P. Anhaus^{1*}, C. Katlein¹, M. Nicolaus¹, M. Hoppmann¹, C. Haas^{1,2}**

5

6 ¹Alfred-Wegener-Institut Helmholtz-Zentrum für Polar- und Meeresforschung, Bremerhaven,
7 Germany

8 ²Department of Environmental Physics, University of Bremen, Bremen, Germany

9

10 *Corresponding author: Philipp Anhaus (philipp.anhaus@awi.de)

11

12 **Key Points:**

- 13 • Thicker snow cover may develop on refrozen melt ponds compared to bare sea ice due to
14 their recessed topography
- 15 • Light transmittance through melt ponds can be lower than through bare sea ice
- 16 • Reduced light transmittance impacts sea ice energy balance and growth and the
17 distribution of under-ice algae

18

19 **Word count = 3618**

20

21 **Abstract**

22 The evolution of melt ponds on Arctic sea ice has a large impact on the surface energy balance
23 and the ice-associated ecosystem. Melt ponds are considered as bright windows to the ocean,
24 because they transmit more solar radiation into the ocean than bare ice, also during freeze-up. Here
25 we present results from under-ice radiation measurements close to the North Pole during summer
26 2018 using a remotely operated vehicle in combination with ice and snow measurements. Our
27 results reveal that light transmittance of melt ponds is lower compared to bare ice once covered by
28 the first snow. Results from a radiative transfer model suggest that refrozen melt ponds with a
29 snow cover (> 0.04 m) lead to lower light transmittance than adjacent bare ice. This has
30 implications on autumn ecosystem activity and thermodynamical ice growth, because it reduces
31 the solar heat input to the Arctic Ocean in September by $>50\%$.

32

33 **Plain Language Summary**

34 Arctic sea ice is covered with melt ponds during summer. These ponds control most of the sunlight
35 and energy that enters the ice-ocean system. The light availability underneath Arctic sea ice with
36 lots of melt ponds is usually much higher than underneath bare ice, also during autumn when the
37 surface refreezes again. Using a robot operated underneath the sea ice close to the North Pole in
38 summer 2018, we discovered a situation where less light was available beneath refrozen melt
39 ponds. We found that the main reason for this opposing behavior is a thicker snow cover on the

40 refrozen pond surface compared to bare ice. This is a surprising finding, because it contradicts the
41 established theory and how it is described in most computer models and theories. It has
42 consequences for our understanding of the ice-associated ecosystem (organisms that live in and
43 under sea ice). It also changes the mass and energy balance of central Arctic sea ice during
44 summer-autumn transition when new sea ice starts forming.

45

46 **1 Introduction**

47 Melt ponds play a key role for the surface energy budget (Nicolaus et al., 2012) and the mass
48 balance of sea ice (Flocco et al., 2015), as well as for the ice- and ocean-associated ecosystem
49 (Arrigo, 2014). During summer, the areal fraction of melt ponds on Arctic first-year ice is up to
50 53% and 20-38% on multi-year ice (Webster et al., 2015; Nicolaus et al., 2012; Fetterer and
51 Untersteiner, 1998). The fraction of the ponds has also been observed to increase (Schröder et al.,
52 2014; Rösel and Kaleschke, 2012). The amount of radiation that is reflected back to the atmosphere
53 is significantly reduced for melt ponds compared to bare ice (e.g., Nicolaus et al, 2012). Instead, a
54 considerable amount of radiation is absorbed by and transmitted through melt ponds (e.g., Katlein
55 et al., 2015; Nicolaus et al., 2012; Ehn et al., 2011; Light et al., 2008; 2015). Consequently, the ice
56 underlying the melt ponds warms and can thin faster than bare ice (Flocco et al., 2015; Hanson,
57 1965; Untersteiner, 1961).

58 The translucent melt ponds are often considered as bright windows in Arctic sea ice, even during
59 autumn when their surface refreezes. The formation and occurrence of under-ice phytoplankton
60 blooms are highly dependent on snow and sea ice conditions and, thus, on the under-ice light field
61 (Ardyna et al., 2020). An Arctic-wide increase in the occurrence of the blooms was partly

62 explained by the increasing fraction of melt ponds (Horvat et al., 2017). Lee et al., 2015 showed
63 that ice algal masses accumulate in and under refrozen melt ponds that favor higher light
64 availability. They argue that algal accumulations in autumn can provide an important food source
65 for higher trophic animals before and during winter.

66 Our study shows that the light availability under melt ponds can be less than under adjacent bare
67 ice after snow fall starts in autumn. Using data collected in the Central Arctic close to the
68 geographic North Pole during the transition from summer to autumn in 2018, we investigate the
69 effect of snow accumulated on the refrozen melt ponds on the under-ice light availability. We
70 compare two datasets that represent the summer and autumn conditions, which mainly consist of
71 snow depth and ice thickness measurements, along with aerial images and under-ice transmittance
72 data from a remotely operated vehicle (ROV). We apply a radiative transfer model to calculate an
73 estimate for the snow accumulation threshold necessary for the light level to be lower under melt
74 ponds compared to bare ice.

75

76 **2 Materials and Methods**

77 **2.1 Study Site**

78 The data presented in this study were collected during the Arctic Ocean 2018 MOCCHA – ACAS
79 – ICE campaign (short: AO18) onboard the Swedish icebreaker *Oden*. During this campaign, a
80 temporary ice camp was set up on drifting, ponded multi-year ice close to the geographic North
81 Pole between 14 August and 14 September 2018. Snow depth, total sea ice thickness (ice thickness
82 plus snow depth) and transmitted irradiance were measured in an area of approximately 100 m x
83 100 m (Figure 1). Marker poles (M0 to M23) were deployed under the ice to facilitate ROV
84 navigation and to obtain a better co-location of the data. The mean ice thickness of bare ice was

85 1.9 m and of the ice underlying the melt ponds 1.7 m (Table S2). Melt ponds were on average 0.3
86 m deep. Here we focus on two main datasets: measurements performed between 17 and 24 August
87 represented summer conditions which were characterized by open or only slightly refrozen melt
88 ponds and no snow cover, whereas measurements performed between 13 and 14 September
89 represented autumn conditions which were characterized by refrozen and snow-covered melt
90 ponds.

91

92 **2.2 Under-Ice Transmittance**

93 Horizontal transects of under-ice spectral irradiance were measured by a RAMSES-ACC hyper-
94 spectral radiometer (TriOS GmbH, Rastede, Germany). The radiometer was mounted on a M500
95 ROV (Ocean Modules, Åtvidaberg, Sweden, Katlein et al., 2017). The ROV was lowered into the
96 water through a 2 x 2 m hole in the ice covered by a tent next to the (pristine) study area.

97 The light transmittance was calculated by wavelength-integrating the transmitted irradiance from
98 350 to 920 nm and normalizing by the incident downwelling planar irradiance recorded by an
99 upward-looking reference sensor at the surface. The data were filtered for ROV pitch, roll and
100 depth, and noise was filtered from the spectra. Using the photosynthetically active radiation (400
101 to 700 nm) did not lead to qualitatively different results and conclusions in this work, and is thus
102 not further considered here.

103 For under-ice navigation, the ROV was equipped with an acoustic long baseline positioning system
104 (Pinpoint 1500 Linkquest, San Diego, CA, USA). We manually post-processed the ROV position
105 to remove distortions caused by calibration uncertainties.

106

107 **2.3 Snow Depth and Sea Ice Thickness**

108 Snow depth point measurements with a horizontal spacing of 1 to 3 m and an accuracy of 0.01 m
109 were obtained using a Magna Probe (Snow-Hydro, Fairbanks, AK, USA, Sturm and Holmgren,
110 2018). The GPS position of each measurement was recorded by an integrated GPS with an
111 accuracy of 2.5 m (Sturm and Holmgren, 2018).

112 Total (sea ice plus snow) thickness was determined using a ground-based electromagnetic
113 induction sounding device (GEM-2, Geophex Ltd, Raleigh, NC, USA, Hunkeler et al., 2015) using
114 the in-phase signal at a frequency of 18.33 kHz. The GEM-2 was placed on a sledge and dragged
115 across the study area in a grid pattern at the very end of the campaign. The accuracy of the total
116 thickness measurements is ± 0.1 m (Hunkeler et al., 2015). Finally, ice thickness was calculated
117 from total thickness by subtracting the (interpolated) snow depths. GPS positions of snow depth
118 and ice thickness measurements were subsequently corrected for ice drift using GPS recorders
119 placed at the acoustic transponder locations to enable co-location with the transmittance
120 measurements.

121 In addition, in situ snow depth, ice thickness, draft, freeboard, and melt pond depth were measured
122 in drill holes at the marker locations using a tape measure on 17 August.

123

124 **2.4 Aerial Images**

125 Oblique aerial images were obtained during a helicopter flight on 23 August (summer) and by a
126 drone on 13 September (autumn). Those were used to retrieve the geographic coordinates of the
127 melt ponds. The images were corrected for camera perspective and georeferenced using the marker
128 locations measured by a terrestrial laser scanner (VZ-400i, RIEGL, Horn, Austria). Melt ponds in

129 the image were detected using a simple threshold criterion. All pixels within the study area where
130 $\text{mean}(R,G,B) < 70 + 0.5 \cdot B$ (Katlein et al., 2015) were classified as melt ponds, with R, G, B
131 representing the integer values of the respective channels of the RGB color space (R=700 nm,
132 G=525 nm, B=450 nm). We added a 2 m buffer by image dilation to account for horizontal light
133 spreading (Ehn et al., 2011) and uncertainties of the ROV position.

134

135 **2.5 Radiative Transfer Model**

136 We modelled under-ice broadband transmittance using the radiative transfer model DORT2002
137 version 3.0 (Edström, 2005; Katlein et al., 2021). The model uses a discrete ordinate model
138 geometry and is implemented in the MATLABTM software. The ice geometry was approximated
139 by three layers each for bare ice and melt ponds (Table S1): The bare ice consisted of the interior
140 sea ice underlying a surface scattering layer (SSL) with a freshly fallen snow layer of varying
141 thickness on top. The melt ponds consisted of interior sea ice underlying the melt pond overlain
142 by a snow layer of varying thickness. For simplicity, the situation without any snow will be referred
143 to as “summer” conditions whereas the snow covered scenario is referred to as “autumn”
144 conditions. We used typical inherent optical properties for multi-year ice (Katlein et al., 2021;
145 Perron et al., 2021).

146

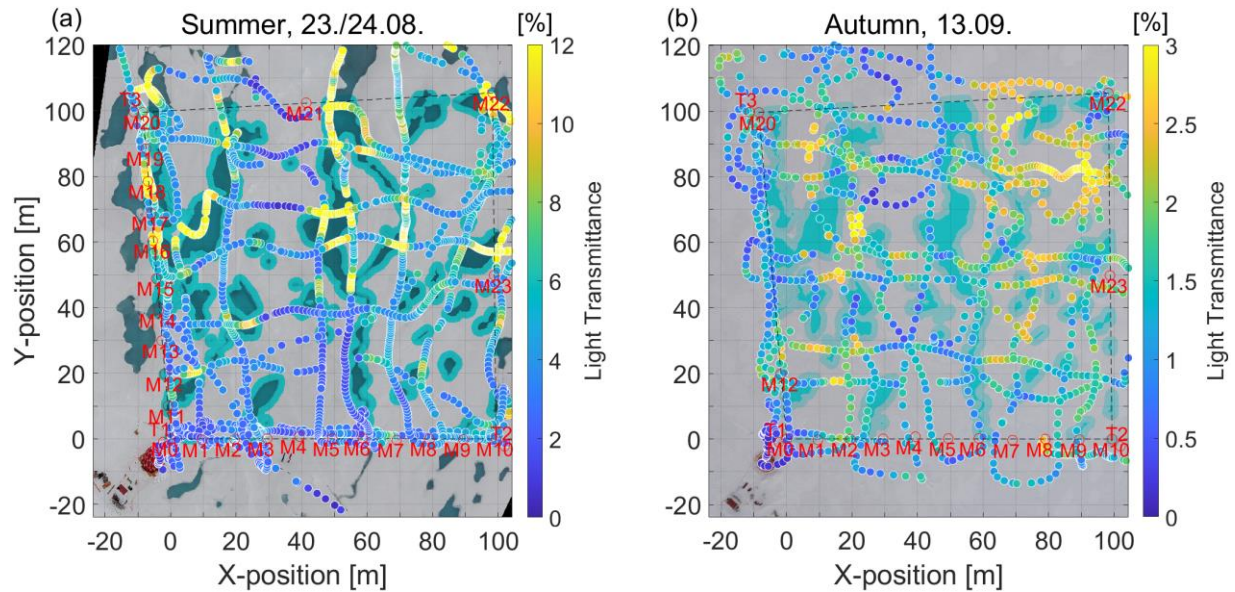
147 **3 Results and Discussion**

148

149 **3.1 Evolution of Surface and Optical Properties in the Transition from Summer to Autumn**

150 Figure 1 illustrates the distribution of melt ponds and bare ice, as well as the magnitude and spatial
 151 variability of under-ice transmittance during the transition from summer to autumn in the study
 152 area.

153



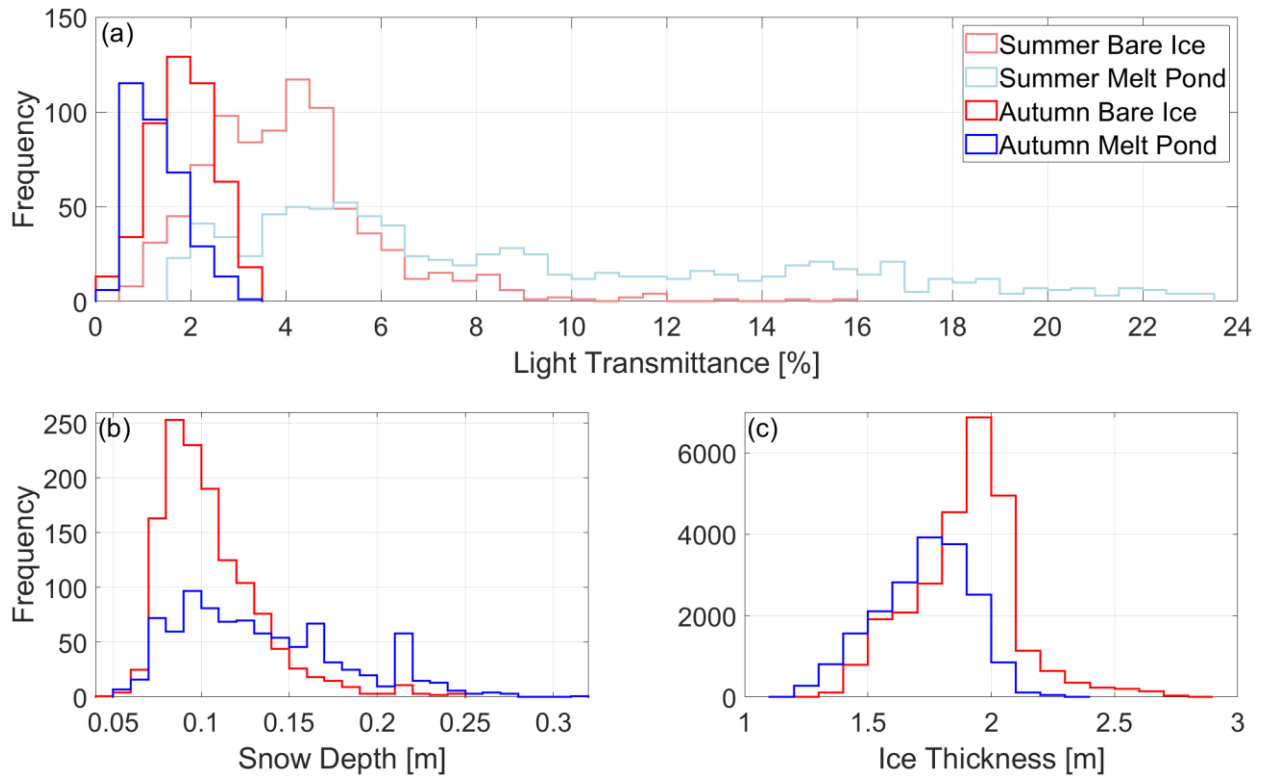
154

155 **Figure 1:** Light transmittance through ponded sea ice during the transition from (a) summer to (b)
 156 autumn. The data show ROV-based radiation measurements under (a) open melts ponds and (b)
 157 refrozen and snow-covered ponds. The background images are orthorectified aerial images
 158 acquired during (a) a low altitude helicopter flight and (b) a drone flight. Pixels within the study
 159 area that were classified as melt pond and used for further analysis are colored in blue. The melt
 160 ponds in (b) were refrozen and snow-covered but marked blue for illustration purposes. The edges
 161 around the melt ponds in (a) and (b) were dilated by a buffer of about 2 m. This area is indicated
 162 by a brighter blue. Red labels indicate the marker (M) and transponder locations (T). The ROV
 163 tent and control hut are visible on the lower left corners of the images. Note the different range in
 164 transmittance in (a) and (b).

165

166 On 23 August, the melt ponds were generally still open but in parts slightly refrozen at the surface
167 (Figures 1a and S1a). The mean and maximum transmittances of ponds (8.9% and 23.2%,
168 respectively) were significantly higher than those of bare ice (4.1% and 15.5%, see also Figure 1a
169 and Table S2) on 24 August. Histograms showed a bi-modal transmittance distribution of ponds
170 and bare ice combined (Figure S2a). The distribution also showed a characteristic long tail for
171 ponds, indicating high spatial variability and different properties of the ponds. This distribution is
172 typical for Arctic summer sea ice and results from the formation and development of the melt
173 ponds (Katlein et al., 2015; 2019; Nicolaus et al., 2012; Schanke et al., 2021). The magnitudes of
174 transmittance are similar to observations from Nicolaus et al. (2012) in the same region in August
175 2011. The maximum transmittance of the melt ponds also agrees to values found by Katlein et al.
176 (2019).

177



178

179 **Figure 2:** Histograms of measured (a) light transmittance, (b) snow depth, and (c) ice thickness of
 180 melt ponds and bare ice.

181

182 After freeze-up, the surface of the melt ponds was refrozen and a snow cover accumulated on top
 183 of it as well as on bare ice (Figure 1b). The transmittance of both melt ponds and bare ice decreased
 184 due to new snow (Figures 1 and S2, Table S2). The spatial variability in the transmittance of both
 185 melt ponds and bare ice was significantly reduced in autumn while the long tail of the high
 186 transmittances diminished, with very few observations higher than 3% (Figures 2a and S2, Table
 187 S2). In summer, approximately 80% (25%) of the transmittance measurements were higher than
 188 3% (9%) while in autumn only 1% (0%). This can be explained by stronger and more frequent
 189 snow fall events that started to occur from 28 August (Vüllers et al., 2021).

190 Lee et al. (2011) describe that melt ponds remain bright windows of Arctic sea ice also in autumn,
191 after refreezing. This implies that the transmittance of melt ponds ice remains higher than that of
192 bare ice. Katlein et al. (2019) showed that the bi-modal structure of transmittance during summer
193 is conserved even during the first weeks of freeze-up in mid of September. They further suggest
194 that the transmittances of both melt ponds and bare ice decrease gradually and equally in the
195 transition from summer to autumn.

196 In contrast to those results, we observed the opposite behaviour: the mean transmittance of melt
197 ponds (1.3 %) was lower than that of bare ice (1.8 %) in autumn (Figures 1b and 2a, Table S2).
198 The transmittance distribution showed two distinct modes of 1.0% and 2.0% associated with melt
199 ponds and bare ice, respectively (Figure 2a, Table S2). This opposing behaviour is explained by
200 the higher mean snow depth (0.14 m) on melt ponds compared to that on bare ice (0.11 m) (Figure
201 2b, Table S2). On the melt ponds, higher snow depths were also much more frequently measured
202 than on bare ice (modes of 0.17 and 0.22 m, Figure 2b).

203 The melt ponds and their recessed topographic position induce a rougher ice surface compared to
204 adjacent bare ice (Figure S1, Fetterer & Untersteiner, 1998). Thus, they provide a catchment area
205 for snow. The passage of low-pressure systems between 29 August and 15 September brought
206 precipitation accompanied by strong winds with speeds up to 13 ms^{-1} (Vüllers et al., 2019). As a
207 result, snow was re-distributed towards and caught by the refrozen melt ponds and their edges,
208 leading to the higher snow accumulation on the ponds.

209 Despite the reversal of the magnitude in the transmittance of melt ponds and bare ice, the spatial
210 variability remained during autumn (Figure 1). This suggests that the spatial variability was still
211 coupled to the ponds after snow accumulation and re-distribution and most likely also persisted
212 into winter.

213 The transmittance of ridged ice with thicknesses up to 2.8 m was naturally still lower than that of
214 the melt ponds (Figures S3b and 1b). Those measurements are included in the bare ice data and
215 are represented in the tail of larger ice thicknesses in the histogram (Figure 2c).

216 This study provides first quantitative observations of lower light transmittance of melt ponds than
217 of bare ice in autumn due to higher snow depths on the ponds. Major implications on the ice-
218 associated ecosystem and the energy and mass balance of the sea ice arise from those observations:

219 Lee et al. (2011) proposed that the soft refrozen surface of open melt ponds that are in connection
220 with the ocean provides a fertile habitat for biomass in autumn. They pointed out that the biomass
221 accumulated under the refrozen melt ponds serves as an important food source for higher trophic
222 animals during the transition from autumn to winter and further into winter. However, as presented
223 here, a snow cover significantly reduces the light availability in and under melt ponds in autumn,
224 suggesting a limited suitability as habitat in terms of available light. Those observations lend
225 support to a study by Lange et al. (2017), who found higher biomass values underneath hummocks
226 on multi-year ice compared to adjacent level ice. Lange et al. (2017) attributed the differences in
227 biomass accumulation to increased light availability under the hummocks resulting from a very
228 thin or absent snow cover. Our results and those of Lange et al. (2017) suggest that light conditions
229 under sea ice in spring can already be initialized by melt pond coverage and snow distribution
230 during autumn and may persist throughout winter.

231 Further, due to the common assumption that there is more light available under melt ponds than
232 under bare ice also during autumn, processes and magnitudes of carbon uptake and biomass
233 accumulation in models, might need to be adjusted with respect to our new observations.

234 Arndt and Nicolaus (2014) developed a parameterization to quantify the annual solar heat input

235 through Arctic sea ice. For their calculations in autumn, they use for transmittances of melt ponds
236 the fivefold (500%) of that of bare ice. However, our results showed that the modal transmittance
237 of melt ponds is only half (50%) of that of bare ice once covered by the first snow (Table S2).
238 Using the parameterization from Arndt and Nicolaus (2014), their constant summer mean melt
239 pond fraction for multi-year ice of 29% (Rösel et al., 2012), their estimate for the solar heat input
240 into the ocean in September of 0.69×10^{19} J, their transmittance of melt ponds on multi-year ice
241 of 0.4%, but the ratio of transmittances between melt ponds and bare ice as presented in the present
242 study, the solar heat input would decrease by 61%. Even though the solar heat input in September
243 is low compared to May-August (e.g., Perovich et al., 2011; Arndt and Nicolaus, 2014), the results
244 of reduced light transmittance of snow-covered melt ponds compared to that of bare ice, should be
245 incorporated in future solar heat input calculations. In this regard, our results might also impact
246 the heat stored in the upper ocean, the interior sea ice structure, as well as internal and basal
247 melting.

248 The implications of our results on the sea ice mass balance are related to the insulating effect of
249 the snow cover. As a consequence, reduced thermodynamic ice growth, delayed freeze-up of the
250 liquid melt pond, and induced bottom roughness are expected.

251 The refrozen surface of the melt ponds alone reduces the heat release from the ocean through the
252 ice towards the atmosphere (Flocco et al., 2015). This hampers ice growth at both water-ice
253 interfaces of the refreezing pond, as well as between the sea ice bottom and the ocean in the
254 transition from autumn to winter. This can result in a delay of the complete freeze-up of the pond
255 by up to 60 days (Flocco et al., 2015). A thinner ice cover is more vulnerable to dynamic and
256 warming events. The presence of a snow cover on top of the refrozen pond surface is expected to
257 amplify those effects. As a result of the reduced thermodynamic growth of the sea ice underlying

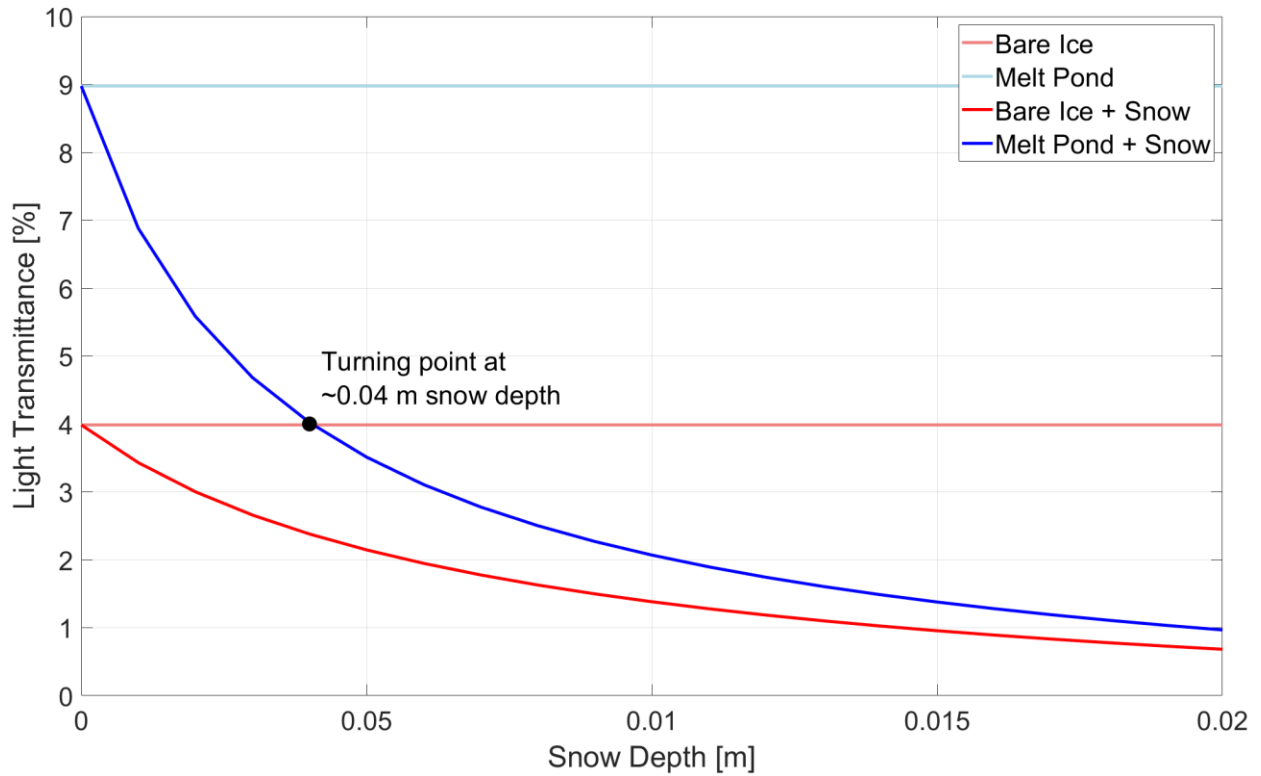
258 melt ponds compared to bare ice, a generally rougher bottom topography might result, affecting
259 the mass, momentum, heat, and salt fluxes at the sea ice-ocean interface.

260 The exact evolution of the optical properties of melt ponds during refreezing depends on the
261 sequence of weather events. Whether or not more snow accumulates on the refrozen melt ponds
262 than on adjacent bare ice is governed by the wind speed and snow drift regime during and after the
263 snow fall, by the snow properties, and by the roughness of the refrozen surface. Falling and
264 deposited snow needs to be re-distributed before it can accumulate on the topographically recessed
265 and rougher pond surface. Wet and heavy snow sticks easier to the refrozen surface of melt ponds
266 and better resists erosion by wind than low density snow. Further, on very flat, dry and smooth
267 nilas, snow might not accumulate that much compared to surfaces that froze under turbulent
268 conditions and that exhibit a rougher and wetter surface where snow can more easily deposit
269 (Sturm et al., 2002).

270

271 **3.2 Radiative Transfer Model**

272 For the effect described above, it is of interest to quantify the threshold snow depth that is necessary
273 to decrease the transmittance of melt ponds below that of bare ice. In order to determine this
274 threshold depth, we used the radiative transfer model DORT2002. For the situation without snow
275 (summer), both the simulated transmittances of melt ponds and bare ice (9% and 4%, respectively)
276 were very similar to our observations (8.9% and 4.1%, respectively, Figure 3, Table S2).



277

278 **Figure 3:** Simulated light transmittance depending on the snow depth as modelled by DORT2002
 279 for four cases: bare ice (light red), melt ponds (light blue), snow-covered bare ice (red), and snow-
 280 covered melt ponds (blue).

281

282 Incorporating an increasing snow cover from 0 to 0.04 m (autumn), our results yielded an
 283 exponential decrease in the transmittances of both melt ponds and bare ice (Figure 3). For a snow
 284 depth of approximately 0.04 m the transmittance of the melt ponds becomes lower than that of
 285 snow-free, bare ice (Figure 3). This is in agreement with the observations presented earlier in this
 286 study which showed that the transmittance of melt ponds was lower than that of bare ice for a 0.03
 287 m higher mean snow depth on the ponds (Table S2).

288 In our simulations, the influence of the thin ice lid on the melt ponds on the transmittance was

289 neglected, as they were only partially existing, as for typical Arctic summer sea ice these are very
290 translucent and scattering is small (Lu et al., 2018), indicated by their blue-green color (Figure 1a).

291

292 **5 Summary**

293 We measured light transmittance under a ponded sea ice floe in the transition from summer to
294 autumn using a ROV together with snow depth and ice thickness and used a radiative transfer
295 model to quantify a threshold snow depth. Those measurements showed that melt ponds cannot be
296 universally considered as bright windows of Arctic autumn sea ice. The transmittance of refrozen
297 melt ponds on Arctic sea ice during autumn can become lower than that of adjacent bare ice. The
298 reason for that is a 0.03 - 0.04 m thicker snow cover that accumulate on the ponds due to their
299 recessed topographic position compared to bare ice. This conclusion has consequences for the ice-
300 associated ecosystem, the thermodynamic sea ice growth and the energy budget. Algae might not
301 dwell as much under the darker melt ponds and we speculate that the snow cover on top of the
302 refrozen ponds hampers ice growth due to its insulating effect and, thus, induces increased bottom
303 roughness.

304

305 **Acknowledgments**

306 This work was financed through the research programs PACES II and POF4 from the Alfred-
307 Wegener-Institut Helmholtz-Zentrum für Polar- und Meeresforschung (AWI) and Swedish Polar
308 Research Secretariat (SPRS, grant no. AO18). Additional funding was received through the
309 Diatom-ARCTIC project (NE/R012849/1; 03F0810A), part of the Changing Arctic Ocean
310 program (CAO), jointly funded by the UKRI Natural Environment Research Council (NERC) and
311 the Bundesministerium für Bildung und Forschung (BMBF). The ROV work was supported by

312 the Helmholtz Infrastructure Initiative Frontiers in Arctic marine Monitoring (FRAM).
313 Participation in the AO18 expedition of the Swedish icebreaker *Oden* was facilitated by SPRS and
314 the AWI logistics. We want to thank in particular Matthieu Labaste, Helen Czerski and Lars
315 Lehnert for their outstanding field support.

316

317 **Data availability**

318 All data presented in this study are publicly available under the following DOIs:

319 ROV: <https://doi.org/10.1594/PANGAEA.925698>

320 Magna Probe and GEM2: DOI generation is currently in progress

321 Aerial images: <https://doi.org/10.5281/zenodo.5119094>

322

323 **Competing interest**

324 The authors declare that they have no conflict of interest.

325

326 **References**

- 327 Ardyna, M., Mundy, C. J., Mills, M. M., Oziel, L., Grondin, L. L., Verin, G., et al. (2020).
328 Environmental drivers of under-ice phytoplankton bloom dynamics in the Arctic Ocean.
329 *Elementa: Science of the Anthropocene*, 8(30). doi:10.1525/elementa.430
- 330 Arndt, S., & Nicolaus, M. (2014). Seasonal cycle and long-term trend of solar energy fluxes
331 through Arctic sea ice. *The Cryosphere*, 8(6). doi:10.5194/tc-8-2219-2014
- 332 Arrigo, K. R. (2014). Sea ice ecosystems. *Annual Review of Marine Science*, 6(1).
333 doi:10.1146/annurev-marine-010213-135103
- 334 Edström, P. (2005). A Fast and Stable Solution Method for the Radiative Transfer Problem. *SIAM*
335 *Rev.*, 47(3). doi:10.1137/s0036144503438718
- 336 Ehn, J. K., Mundy, C. J., Barber, D. G., Hop, H., Rossnagel, A., & Stewart, J. (2011). Impact of
337 horizontal spreading on light propagation in melt pond covered seasonal sea ice in the
338 Canadian Arctic. *Journal of Geophysical Research*, 116. doi:10.1029/2010jc006908
- 339 Fetterer, F., & Untersteiner, N. (1998). Observations of melt ponds on Arctic sea ice. *Journal of*
340 *Geophysical Research: Oceans*, 103(C11). doi:10.1029/98jc02034

- 341 Flocco, D., Feltham, D. L., Bailey, E., & Schroeder, D. (2015). The refreezing of melt ponds on
342 Arctic sea ice. *Journal of Geophysical Research: Oceans*, *120*(2).
343 doi:10.1002/2014jc010140
- 344 Hanson, A. (1965). Studies of the Mass Budget of Arctic Pack-Ice Floes. *Journal of Glaciology*,
345 *5*(41). doi:10.3189/S0022143000018694
- 346 Hunkeler, P. A., Hoppmann, M., Hendricks, S., Kalscheuer, T., & Gerdes, R. (2016). A glimpse
347 beneath Antarctic sea ice: Platelet layer volume from multifrequency electromagnetic
348 induction sounding. *Geophysical Research Letters*, *43*(1), 222-231.
349 doi:10.1002/2015gl065074
- 350 Katlein, C., Arndt, S., Nicolaus, M., Perovich, D. K., Jakuba, M. V., Suman, S., et al. (2015).
351 Influence of ice thickness and surface properties on light transmission through Arctic sea
352 ice. *Journal of Geophysical Research: Oceans*, *120*(9). doi:10.1002/2015JC010914
- 353 Katlein, C., Schiller, M., Belter, H. J., Coppolaro, V., Wenslandt, D., & Nicolaus, M. (2017). A
354 New Remotely Operated Sensor Platform for Interdisciplinary Observations under Sea Ice.
355 *Frontiers in Marine Science*, *4*. doi:10.3389/fmars.2017.00281
- 356 Katlein, C., Arndt, S., Belter, H. J., Castellani, G., & Nicolaus, M. (2019). Seasonal Evolution of
357 Light Transmission Distributions Through Arctic Sea Ice. *Journal of Geophysical
358 Research: Oceans*, *124*(8). doi:10.1029/2018jc014833
- 359 Katlein, C., Valcic, L., Lambert-Girard, S., & Hoppmann, M. (2021). New insights into radiative
360 transfer within sea ice derived from autonomous optical propagation measurements. *The
361 Cryosphere*, *15*(1). doi:10.5194/tc-15-183-2021
- 362 Lange, B. A., Flores, H., Michel, C., Beckers, J. F., Bublitz, A., Casey, J. A., et al. (2017). Pan-
363 Arctic sea ice-algal chl a biomass and suitable habitat are largely underestimated for
364 multiyear ice. *Global Change Biology*, *23*(11). doi:10.1111/gcb.13742
- 365 Lee, S. H., McRoy, C. P., Joo, H. M., Gradinger, R., Cui, H., Yun, M. S., et al. (2011). Holes in
366 Progressively Thinning Arctic Sea Ice Lead to New Ice Algae Habitat. *Oceanography*,
367 *24*(3). doi:10.5670/oceanog.2011.81
- 368 Light, B., Grenfell, T. C., & Perovich, D. K. (2008). Transmission and absorption of solar radiation
369 by Arctic sea ice during the melt season. *Journal of Geophysical Research*, *113*(C03023).
370 doi:10.1029/2006jc003977
- 371 Light, B., Perovich, D. K., Webster, M. A., Polashenski, C., & Dadic, R. (2015). Optical properties
372 of melting first-year Arctic sea ice. *Journal of Geophysical Research: Oceans*, *120*(11).
373 doi:10.1002/2015jc011163
- 374 Lu, P., Cao, X., Wang, Q., Leppäranta, M., Cheng, B., & Li, Z. (2018). Impact of a Surface Ice
375 Lid on the Optical Properties of Melt Ponds. *Journal of Geophysical Research: Oceans*,
376 *123*(11). doi:10.1029/2018jc014161
- 377 Nicolaus, M., Katlein, C., Maslanik, J., & Hendricks, S. (2012). Changes in Arctic sea ice result
378 in increasing light transmittance and absorption. *Geophysical Research Letters*, *39*(24).
379 doi:10.1029/2012gl053738
- 380 Perovich, D. K., Richter-Menge, J. A., Jones, K. F., Light, B., Elder, B. C., Polashenski, C., et al.
381 (2011). Arctic sea-ice melt in 2008 and the role of solar heating. *Annals of Glaciology*,
382 *52*(57). doi:10.3189/172756411795931714
- 383 Perron, C., Katlein, C., Lambert-Girard, S., Leymarie, E., Guinard, L.-P., Marquet, P., et al. (2021).
384 Development of a Diffuse Reflectance Probe for In Situ Measurement of Inherent Optical
385 Properties in Sea Ice, *The Cryosphere Discuss.*, in review, doi:10.5194/tc-2021-104

- 386 Rösel, A., & Kaleschke, L. (2012). Exceptional melt pond occurrence in the years 2007 and 2011
387 on the Arctic sea ice revealed from MODIS satellite data. *Journal of Geophysical*
388 *Research: Oceans*, 117(C05018). doi:10.1029/2011jc007869
- 389 Rösel, A., Kaleschke, L., & Birnbaum, G. (2012). Melt ponds on Arctic sea ice determined from
390 MODIS satellite data using an artificial neural network. *The Cryosphere*, 6(2).
391 doi:10.5194/tc-6-431-2012
- 392 Schröder, D., Feltham, D. L., Flocco, D., & Tsamados, M. (2014). September Arctic sea-ice
393 minimum predicted by spring melt-pond fraction. *Nature Climate Change*, 4(5).
394 doi:10.1038/nclimate2203
- 395 Sturm, M., Holmgren, J., & Perovich, D. K. (2002). Winter snow cover on the sea ice of the Arctic
396 Ocean at the Surface Heat Budget of the Arctic Ocean (SHEBA): Temporal evolution and
397 spatial variability. *Journal of Geophysical Research*, 107(C10).
398 doi:10.1029/2000jc000400
- 399 Sturm, M., & Holmgren, J. (2018). An Automatic Snow Depth Probe for Field Validation
400 Campaigns. *Water Resources Research*, 54(11). doi:10.1029/2018wr023559
- 401 Untersteiner, N. (1961). On the Mass and Heat Budget of Arctic Sea Ice. *Archiv für Meteorologie,*
402 *Geophysik und Bioklimatologie, Serie A*, 12. doi:10.1007/BF02247491
- 403 Vüllers, J., Achtert, P., Brooks, I. M., Tjernström, M., Prytherch, J., Burzik, A., et al. (2021).
404 Meteorological and cloud conditions during the Arctic Ocean 2018 expedition.
405 *Atmospheric Chemistry and Physics*, 21(1). doi:10.5194/acp-21-289-2021
- 406 Webster, M. A., Rigor, I. G., Perovich, D. K., Richter-Menge, J. A., Polashenski, C. M., & Light,
407 B. (2015). Seasonal evolution of melt ponds on Arctic sea ice. *Journal of Geophysical*
408 *Research: Oceans*, 120(9). doi:10.1002/2015jc011030
- 409